base and hence a large spall fragment travel time, during which the disturbing influence of the target edges, located in the unloading zone, may make itself felt. This factor can lead to a lower value of the real spall velocity as compared with ideal experimental conditions. Since these edge effects are not usually monitored during the experiment, they can lead to unverifiable errors in calculating the spall strength from Eq. (2).

Thus, in cases where the shear strength or relaxation processes cannot be neglected, using Eq. (1) may lead to appreciable errors in determining the spall strength of the material. The use of Eq. (2) is justified only under special loading conditions, which are different for each specific type of equation of state.

LITERATURE CITED

1. S. A. Novikov, I. I. Divnov, and A. G. Ivanov, "Investigation of the fracture of steel, aluminum and copper under explosive loading," Fiz. Met. Metalloved., 21, No. 4 (1966).
2. A. G. Ivanov and S. A. Novikov, "Capacitive transducer method of recording the instantaneous velocity of a moving surface," Prib. Tekh. Eksp., No. 1 (1963).
3. R. Courant and K. O. Friedrichs, Supersonic Flow and Shock Waves, Wiley-Interscience, New York (1948).
4. L. E. Malvern, "The propagation of longitudinal waves of plastic deformation in a bar exhibiting a strain rate effect," Q. Appl. Math., 8, 405 (1951).

EXPERIMENTAL – THEORETICAL INVESTIGATION OF THE REBOUND OF SHORT RODS FROM A RIGID BARRIER

V. M. Boiko, A. I. Gulidov, A. N. Popyrin, V. M. Fomin, and Yu. A. Shitov

UDC 538.374

The present paper is a natural continuation of [1, 2], which gave a numerical simulation of the rebound of short homogeneous cylindrical and conical rods in the two-dimensional formulation. The integral criterion introduced in connection with the determination of the moment of rebound is applied not only to homogeneous rods but also to rods composed of different materials. The results of the numerical simulation are compared with the experimental data.

1. The physicomathematical formulation of impact problems, the definition of rebound, and the boundary and initial conditions were given in [1, 2] for homogeneous rods. We will now consider the case of a cylindrical rod composed of different materials impacting against a rigid barrier.

Problem 1. A cylindrical rod of length L_0 and radius R_0 consists of two materials. The materials are arranged in layers parallel to the axis of symmetry. The inner cylinder has the radius $R_0/2$. The thickness of the outer sheath is also $R_0/2$. The impact velocity $v_0 = 50$ m/sec. At the boundary between the layers the condition of perfect mechanical contact is satisfied. Mathematically, this condition reduces to the equality of the displacements and stresses at this boundary.

We will find the solution of the problem by the modified Wilkins method [2, 3]. In the numerical solution of the problem the calculation proceeds without explicit identification of the interface. The calculations were made for steel and copper layers with constants: $\rho_0 = 7.85$ g/cm^3, $k = 170$ GPa, $\mu = 80$ GPa, $y_0 = 1.2$ GPa – steel; $\rho_0 = 8.9$ g/cm^3, $k = 139$ GPa, $\mu = 46$ GPa, $y_0 = 0.3$ GPa – copper, where ρ_0 is the density of the material, k is the bulk modulus, μ is the shear modulus, and y_0 is the yield point.

Figure 1 shows the force acting at the rod–barrier interface as a function of time t for four combinations of materials (1 and 4 – solid steel and solid copper, respectively; 2 – inner cylinder copper, outer sheath steel; 3 – inner cylinder steel, outer sheath copper). We note that for the same initial impact velocity and the same geometry, the mass of the rods will be different and hence so will be the initial kinetic energy of the rods.

Novosibirsk. Translated from Zhurnal Prikladnoi Mekhaniki i Tekhnicheskoi Fiziki, No. 5, pp. 129-133, September-October, 1982. Original article submitted January 27, 1981.

0021-8944/82/2305-0705$07.50

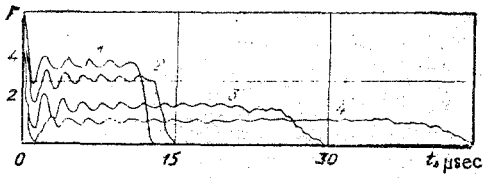

Fig. 1

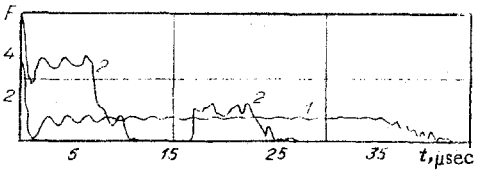

Fig. 2

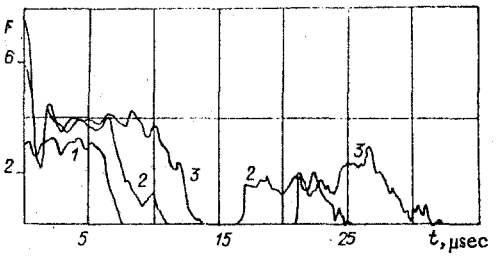

Fig. 3

However, only the yield point of the materials has a significant effect on the rod–barrier contact time t_c: The lower the yield point the greater the rod–barrier contact time (cases 1 and 4). The nature of this effect is as follows: On impact a compression shock of two-wave configuration is propagated from the contact surface. The elastic precursor travels at the elastic wave velocity, which considerably exceeds the plastic wave velocity. On reflection from the free end of the rod the elastic compression wave goes over into a tension wave and is propagated in the opposite direction. The interaction of these waves is associated with a stress redistribution which leads to a decrease in the stress level behind the plastic wave front. The result of this interaction is again an elastic compression wave, with amplitude corresponding to the yield point of the material, moving in the direction of the free end of the rod. As a result of several interactions between the unloading and plastic waves the stresses in the latter decrease and, in the end, become tensile. This leads to the separation of the rod from the barrier. Thus, as the yield point of the material increases, so does the amplitude of the unloading wave, and the compressive stresses in the rod are relieved after fewer interactions between the unloading and plastic waves.

For a composite rod, the contact time will be greater in case 3 than in case 2, and the stress level will be higher in the rod consisting of a copper cylinder in a steel sheath. Clearly, moreover, in this case the total deformation of the rod will be less.

Problem 2. The geometric dimensions of the rod remain the same as in Problem 1. The impact velocity $v_0 = 50$ m/sec. The materials are as before, but arranged so that one half of the rod, of length L/2, is of one material and the other. Impact is assumed to be first at the copper end, then at the steel end. In Fig. 2 the force F is shown as a function of time t for these two variants.

In case 1 the contact time is close to that for a solid copper rod, and the F(t) graph resembles graph 4 in Fig. 1.

In the second case (impact at the steel end) after the force F has fallen to zero and the rod has rebounded, there is a second contact with the barrier. We will call this effect double rebound. If the impact velocity is increased, then the first rebound time increases, but at the same time there is an increase in the second contact time and in the interval between first rebound and second contact. In Fig. 3 we have plotted F(t) for three values of the initial impact velocity: 25, 50, and 75 m/sec. It is noteworthy that the time interval between the first rebound and the second contact depends on the ratio of the lengths of the steel and copper segments of the rod. It was found that when the copper segment has a certain length second contact does not occur. In this case the overall length of the rod remains the same. The explanation of the double rebound effect is similar to the explanation of the behavior of a solid rod. Here it is necessary to take into consideration the fact that at the steel–copper interface there is a redistribution of stresses in the compression wave, since the interaction between the latter and the contact surface leads to the formation of a rarefaction wave traveling into the steel part of the rod. This is because copper is softer than steel.

2. For the experimental observation of the collision process we developed a high-speed photorecording technique which makes it possible to determine such parameters as the velocity and penetration rate, contact time, etc. Obviously, in recording processes taking place at a velocity of around 10^3 m/sec, it is necessary

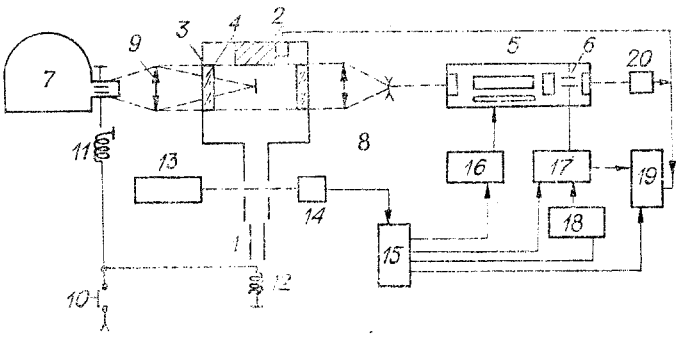

Fig. 4

to employ high-speed apparatus (frame exposure around 10^{-7} sec). Most promising from this standpoint are optical multiexposure photorecording systems based on laser light sources. The use of a series of short controlled laser pulses makes it possible to obtain good spatial and time resolution and ensure strict synchronization with the investigated phenomenon.

In our case we constructed a stroboscopic light pulse source based on a ruby laser with periodic Q-switching [4], which made it possible to obtain a series of pulses (from 1 to 100) lasting $\approx 3 \times 10^{-8}$ sec. The intervals between pulses could be regulated discretely, in steps of 1 μsec, on the range from 10 to 500 μsec, with an accuracy of 0.2 μsec. A Kerr cell was used as the electrooptic modulator. The active medium was a ruby crystal 8 mm in diameter and 120 mm long. The resonator was composed of two mirrors with dielectric coatings. A mirror with a reflection coefficient of ~100%, together with the Q-switch, formed a quarter-wave shutter-reflector actuated by the voltage drop. As the polarizer we used an Iceland spar prism. The quarter-wave shutter-reflector was designed as a unit and mounted in a fluoroplastic housing filled with nitrobenzene. The parameters of the Kerr cell were as follows: electrode spacing 8 mm, electrode length 50 mm, quarter-wave voltage 15 kV, cell capacitance 30 pF. The electronic control circuit of the Kerr cell consisted of: (1) synchronizing pulse generator. For this purpose we used an ordinary GZ4-6 six-channel delayed pulse generator; 2) master oscillator, generating a series of electric pulses varying in number from 1 to 10^3 and separated by intervals that can be regulated discretely, in steps of 1 μsec, on the range from 2 to 10^3 μsec. As the master oscillator we used a G5-27 industrial oscillator with an accurately calibrated time lag. The presence of a quartz resonator ensured a pulse interval instability of not worse than 0.1 μsec; 3) high-voltage pulse shaper.

The experimental setup is illustrated in Fig. 4. To obtain the necessary rod velocity (cylinder, diameter $2R_0 = 5.2$ mm, length $L_0 = 20$ mm) we used an accelerating device 1. The barrier 2 was mounted in a protective steel chamber 3 with transparent windows 4. The collision process was recorded using high-speed motion-picture photography. As the stroboscopic light source we used a laser 5 with periodic Q-switching by means of a quarter-wave Kerr shutter 6. The image was registered by a ZhFR-3 slave photorecorder 7 operating in the photoscanning mode. A telescopic system 8 expanded the laser beam to the dimensions of the window (d = 60 mm), and by means of a lens 9 (focal length f = 300 mm) an image of the projectile and barrier was focused on the photorecorder film. The apparatus worked as follows: The laser stroboscope pumping lamp battery was charged, and the projectile placed in the accelerator. The electromechanical shutter 11 of the photorecorder was opened by means of the "start" button 10, and the accelerator was triggered by means of the electromagnetic starter 12. On its way to the target the rod cut the beam of the LG-52-3 laser 13 used for synchronization purposes, whereupon a signal of negative polarity was transmitted from an FD-2 photodiode 14 to the GZI-6 synchropulse generator 15. With preselected delays synchropulses were transmitted from the GZI-6 to the laser pumping lamp ignition unit 16, the high-voltage pulse shaper 17, and the master oscillator 18. The number and shape of the pulses were checked by means of a S8-2 storage oscillograph 19; in this case the electric pulses from the Kerr cell are transmitted across a capacitive divider to one input of the oscillograph and the light pulses, converted to electric pulses by an FÉK-14 photocell 20, to the other. The oscillograph also received the signals from a strain transducer attached to the barrier 2.

The same apparatus was also used for recording the collision process in the slit scanning mode. A control voltage was not supplied in the Kerr cell, and the laser operated in the free-running mode. The operation of the laser was monitored by means of the S8-2 oscillograph. At the same time, time marks were transmitted to the oscillograph from the master oscillator.

The motion-picture record of the collision process shown in Fig. 5a was obtained in the framing mode. The interval between frames was 40 μsec, the exposure 3×10^{-8} sec. The photograph reproduced in Fig. 5b was

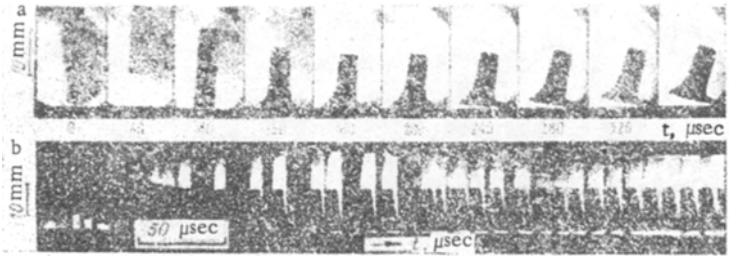

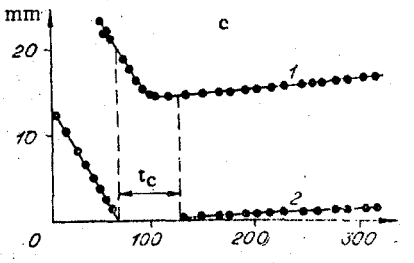

Fig. 5

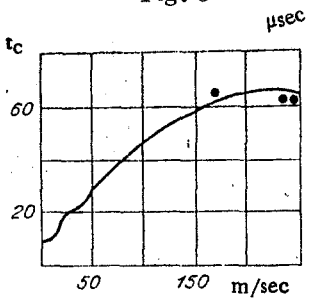

Fig. 6

taken in the photoscanning mode with the laser operating in the spike mode. From these photographs it is possible to determine the flight and rebound velocities of the rod, together with the contact time. A typical velocity graph for the two ends of a cylindrical copper rod in collision with a steel barrier is shown in Fig. 5c (1 – trailing end of rod, 2 – leading end).

In Fig. 6 the numerical calculations are compared with experiment. The continuous curve represents the dependence of the contact time on initial impact velocity for a copper rod and a steel barrier. The impact of the rod against the rigid barrier was calculated using the following parameters: length and diameter of rod 2 and 0.55 cm, respectively, density of material $\rho_0 = 8.9$ g/cm^3, bulk modulus k = 139 GPa, shear modulus $\mu = 46$ GPa. It was assumed that the dynamic yield point of copper $y_0 = 0.3$ GPa. As distinct from the impact problem for a steel rod [2], the interval of stepwise behavior t_* is displaced into the initial region of the curve at impact velocities up to 20 m/sec. This is because, as the impact velocity increases, the amplitude of the stresses in the plastic wave increases more rapidly for copper than for steel. The results of the experiments to determine the contact time in a collision between a copper rod and a hardened steel barrier are presented in Fig. 6 (points).

The satisfactory agreement between calculation and experiment indicates that the mathematical model of the elastoplastic behavior of the medium correctly describes the rebound of the rod from the barrier.

LITERATURE CITED

1. A. I. Gulidov and V. M. Fomin, "Analysis of the propagation of elastoplastic waves in short rods," in: Mater. Symp. "Nonlinear Deformation Waves," Part II [in Russian], Tallinn (1978).
2. A. I. Gulidov and V. M. Fomin, "Numerical simulation of the rebound of axisymmetric rods from a rigid barrier," Zh. Prikl. Mekh. Tekh. Fiz., No. 3 (1980).
3. M. Wilkins, "Calculation of elastoplastic flows," in: Computational Methods in Hydrodynamics [Russian translation], Mir, Moscow (1967).

4. V. M. Boiko and A. N. Papyrin, "High-speed laser diagnostics of heterogeneous flows," in: Modern Experimental Methods of Investigating Heat and Mass Transfer Processes, Part 2 [in Russian], Institute of Heat and Mass Transfer, Academy of Sciences of the Belorussian SSR, Minsk (1981), pp. 3-20.

PROPAGATION OF ONE-DIMENSIONAL ELASTOPLASTIC WAVES IN SOILS

N. Mamadaliev and A. I. Yusupov

UDC 539.374.534.1

In the present article, proceeding from stress–strain theory [1], we investigate the distribution of a plane and a spherical wave in an elastoplastic medium. The stress–strain state of the medium is characterized by the displacement $u(r, t)$, the strains $\varepsilon_{rr} = \partial u/\partial r$, $\varepsilon_{\varphi\varphi} = \varepsilon_{\theta\theta} = u/r$ ($\varepsilon_{\varphi\varphi} = \varepsilon_{\theta\theta} = 0$ in the planar case), and the stresses σ_{rr}, $\sigma_{\varphi\varphi} = \sigma_{\theta\theta}$. We show that either a shock wave or continuous loading–unloading waves can occur in the medium (soil), depending on the forms of the constitutive functions $\sigma(\varepsilon)$, $\sigma_i(\varepsilon_i)$ in the theory of [1]. The indicated waves in soils are investigated in the case $\sigma = (\alpha_1 + \alpha_2|\varepsilon|)\varepsilon$, $\sigma_i = (\beta_1 - \beta_2\varepsilon_i)\varepsilon_i$, where α_i, β_i ($i = 1, 2$) are positive constant coefficients. The solutions of the problems are obtained by an inverse approach [2, 3] with the geometry of the wave surface specified by a second-degree polynomial with respect to the time t (for a shock wave) or the coordinate r (for an unloading wave). It is assumed that the unloading process of the medium is irreversible and linear both with respect to the hydrostatic pressure σ with respect to the stress intensity σ_i. The parameters of the medium, including the load profile, are calculated on a computer on the basis of the derived analytical equations, and the results are presented as graphs of the components of the stresses and particle velocity. We also analyze the case $\sigma_i = \sigma_i(\varepsilon, \varepsilon_i)$ with regard for possible wave effects and the mutual influence of the first and second invariants of the stress or strain tensor. This study represents a continuation of [4] to the case where the strength characteristics of the medium are incorporated in the analysis of the dynamics of transient processes.

We note that problems in the propagation of a plane and a spherical wave have been studied previously by many authors, specifically in [5-14]. However, the soil and rock models used in those works differ considerably from [1]. For example, stress–strain theory is used in [5, 14], the constitutive equations of plastic flow [16] are used in [6-8], the theory of soil plasticity [17] is used in [9, 10], etc.

In contrast with [5-14], for our solution of the above-indicated problems we describe the motion and state of the medium under dynamic loading by the equations of the stress–strain theory of soil plasticity [1], demonstrate the existence of a plane unloading wave for a triaxial stressed state of the medium, and give detailed comparisons of the parameters of an elastoplastic medium and a generalized "plastic gas." We investigate the characteristic features of the propagation of a spherical wave in an elastoplastic medium and the behavior of its parameters for strong disturbances of an explosive nature.

1. Let an instantaneously initiated and then arbitrarily decaying load $\sigma_0(t)$ act along the normal to some plane. In this situation the equation of motion of the medium and the relations between the stresses and strains [1] with regard for the unloading theorem of Il'yushin [15] have the form

$$\rho_0 \partial^2 u/\partial t^2 = \partial \sigma_{rr}/\partial r; \tag{1.1}$$

in loading

$$\begin{gathered} \sigma_{rr} = (\lambda + 2G)\varepsilon, \quad \sigma_{\varphi\varphi} = \sigma_{\theta\theta} = \lambda\varepsilon, \quad \lambda = \sigma/\varepsilon - (2/9)\sigma_i/\varepsilon_i, \\ G = (1/3)\sigma_i/\varepsilon_i, \\ \sigma = (\alpha_1 + \alpha_2|\varepsilon|)\varepsilon, \quad \sigma_i = (\beta_1 - \beta_2\varepsilon_i)\varepsilon_i; \end{gathered} \tag{1.2}$$

in unloading

$$\begin{gathered} \sigma_{rr} - \sigma_{rr}^* = (\lambda_0 + 2G_0)(\varepsilon - \varepsilon^*), \\ \sigma_{\varphi\varphi} - \sigma_{\varphi\varphi}^* = \lambda_0(\varepsilon - \varepsilon^*), \quad \lambda_0 = E_1 - \frac{2}{9}E_2, \quad G_0 = \frac{1}{3}E_2, \end{gathered} \tag{1.3}$$

Moscow. Karshi. Translated from Zhurnal Prikladnoi Mekhaniki i Tekhnicheskoi Fiziki, No. 5, pp. 133-142, September-October, 1982. Original article submitted June 3, 1981.

0021-8944/82/2305-0709$07.50